THE ASTROPHYSICAL JOURNAL, 210:184–198, 1976 November 15

THE EVOLUTION OF ROTATING STARS. I. METHOD AND EXPLORATORY CALCULATIONS FOR A 7 $M_\odot$ STAR

A. S. ENDAL*
Laboratory for Optical Astronomy, NASA, Goddard Space Flight Center
AND
S. SOFIA†
NASA Headquarters
Received 1976 January 16

ABSTRACT

A method is developed which allows us to study the evolution of rotating stars well beyond the main-sequence stage. We consider four different cases of redistribution of angular momentum in an evolving star. Evolutionary sequences for a 7 $M_\odot$ star, rotating according to these different cases, were computed from the zero-age main sequence to the double shell source stage. Each sequence was begun with a (typical) equatorial rotational velocity of 210 km s^{-1}. On the main sequence, the effects of rotation are of minor importance. However, as the core contracts during later stages, important effects arise in all physically plausible cases. The outer regions of the cores approach critical velocities and develop unstable angular velocity distributions. The effects of these instabilities should significantly alter the subsequent evolution.

Subject headings: stars: evolution — stars: interiors — stars: rotation

I. INTRODUCTION

In the past 20 years, astonishing progress has been made toward understanding stellar evolution. In spite of an enormous number of studies of spherical models, however, relatively little attention has been paid to the role of rotation. Basically, there are two reasons for the neglect of rotation in most previous investigations: first, dropping the assumption of spherical symmetry leads to a substantial increase in the numerical complexity of the equations of stellar structure; second, spherically symmetric (nonrotating) models have been very successful in explaining the relevant observational data (the mass-luminosity relationship, H-R diagrams of clusters, etc.).

The problem of numerical complexity can be reduced somewhat by using coordinate systems defined in terms of equipotential surfaces. This will be discussed further in § II. The success of spherical stellar evolution theory can be understood by considering the stages of evolution to which most observational tests apply, i.e., the main sequence (MS) and early post–MS stages. Calculations of rotating MS stars, for example, show that the effects of rotation on the internal structure of such stars are very small, unless the interiors are rotating much more rapidly than the surface layers (see, e.g., Sackmann and Anand 1970; Bodenheimer 1971). Because of the long duration of the MS stage, it is reasonable to expect that various dissipation mechanisms (such as large-scale circulation currents) will reduce any rapid core rotation built up during contraction to the MS, so rotation will not play a significant role during the MS and early post–MS stages.

The situation is very different for the later stages of evolution. Consider the ratio of the centrifugal force, F_c, due to rotation to the force, F_g, due to gravity in the equatorial plane. As successive fuels are exhausted and the core contracts, F_c/F_g will increase in inverse proportion to the radius of the core, if angular momentum is conserved within the core. Redistribution of angular momentum throughout the star is inhibited by the short time scales for the evolution and by large radial gradients in the mean molecular weight, which choke off large-scale circulation currents. Sackmann and Weidemann (1972) and Maeder (1974) have shown that rotation should play a major role in the evolution subsequent to core helium exhaustion, and Sofia (1971) has shown that the rotation rate may be the central parameter in the final gravitational collapse of a star.

Aside from calculations of differentially rotating white dwarfs, which we will not consider since they are not evolutionary sequences, we are aware of only two investigations in which models were calculated well beyond the MS with the effects of rotation included. Kippenhahn, Meyer-Hofmeister, and Thomas (1969, subsequently referred to as KMT) followed the evolution of a 9 $M_\odot$ star from the zero-age main sequence (ZAMS) to the end of helium burning in the core. Two sequences of models were computed, corresponding to two prescriptions of how $\omega(M_r)$, the angular velocity as a function of the mass coordinate, evolves with time. Meyer-Hofmeister (1972) computed sequences for 5, 6, and 9 $M_\odot$ stars through the same

* NAS–NRC Postdoctoral Research Associate.
† On leave from the Department of Astronomy, University of South Florida.

stages of evolution but used only one of the prescriptions for $\omega(M_r)$ used by KMT. In both investigations, spherical symmetry was assumed and the effects of rotation were approximated by taking the radial component of the centrifugal force (averaged over a sphere) into account in the hydrostatic equilibrium equation. As will be discussed in § II, this provides only a rough estimate of the effects of rotation on the evolution.

It appears, therefore, that considerable work remains to be done on the role of rotation in the post–MS stages of evolution. This is the first of a series of papers in which we will systematically explore the effects of rotation on these stages. In this paper, we will concentrate on the computational techniques and describe the results of some sample calculations on the evolution of a $7\,M_\odot$ star from the ZAMS to the double shell source stage, using several different prescriptions for the evolution of $\omega(M_r)$. In § II, we outline the method we use to include the effects of rotation. Comparisons with other methods and numerical tests are described in § III. The starting models and the prescriptions for $\omega(M_r)$ are specified in § IV. The results of the evolutionary calculations are presented in § V and discussed in § VI. A detailed description of the evaluation of the total potential is given in the Appendices.

II. THE EQUATIONS FOR ROTATING STARS

There are four ways in which rotation may affect the equations of stellar structure:

1. Centrifugal forces reduce the effective gravity at any point not on the axis of rotation. This must be taken directly into account in the equation of hydrostatic equilibrium.

2. Because the centrifugal force is not, in general, parallel to the force of gravity, equipotential surfaces are no longer spheres and the spherical relationships between the radius, enclosed volume, and surface area of an equipotential surface cannot be used. This affects all of the equations except the equation for adiabatic convective equilibrium.

3. Because the radiative flux varies with the local effective gravity (the von Zeipel effect), the radiative flux is not constant on an equipotential surface. This enters directly into the radiative equilibrium equation and may affect the stability to convection by changing the radiative temperature gradient.

4. Rotation may inhibit certain modes of convective motions and, thus, directly affect the criterion for convective stability (cf. Randers 1942; Cowling 1951). In addition, not all angular momentum distributions are stable, and this can lead to convection in regions which are stable to purely thermal convection (cf. Wasiutyński 1946).

The first three effects can be incorporated into the equations of stellar structure in a fairly direct manner, if the total (gravitational plus rotational) potential, ψ, is conservative. The formulation we use has been derived by Kippenhahn and Thomas (1970), and we will subsequently refer to this formulation as the KT method. Because the form in which we use the equations is slightly different from that of Kippenhahn and Thomas and in order to clarify how the effects of rotation are taken into account, we rederive the equations here.

The spherical surfaces normally used in stellar models are replaced by equipotential surfaces. The area of such a surface is denoted by S_ψ and the volume enclosed by the surface by V_ψ. On such a surface, the pressure P, the temperature T, and the density ρ are constant, if the total potential is conservative. The Lagrangian coordinate M_r is replaced by M_ψ, the mass interior to the equipotential surface; and the spatial variable r is replaced by r_ψ, the radius of a sphere enclosing a volume V_ψ, i.e.,

$$V_\psi = \frac{4\pi}{3} r_\psi^3 . \tag{1}$$

For any quantity f, which is not constant over an equipotential surface, a mean value is defined by

$$\langle f \rangle = \frac{1}{S_\psi} \int_{\psi = \text{const.}} f d\sigma , \tag{2}$$

where $d\sigma$ is an element of the surface ψ = constant. The local effective gravity is defined by

$$g = d\psi/dn , \tag{3}$$

where dn is the distance between the surfaces ψ = constant and $\psi + d\psi$ = constant. Because of the definition of r_ψ, the form of the mass continuity equation is not altered by rotation:

$$\partial M_\psi = \rho \partial V_\psi = 4\pi r_\psi^2 \rho \partial r_\psi , \tag{4}$$

or

$$\partial r_\psi / \partial M_\psi = 1/4\pi r_\psi^2 \rho . \tag{5}$$

From equation (2),

$$\begin{aligned} \partial V_\psi &= \int_{\psi = \text{const.}} dn d\sigma \\ &= \partial\psi \int_{\psi = \text{const.}} (dn/d\psi) d\sigma = \langle g^{-1} \rangle S_\psi \partial\psi ; \end{aligned} \tag{6}$$

and combining this with equation (4) gives

$$\begin{aligned} \partial\psi &= (\partial V_\psi/\partial\psi)^{-1} \partial V_\psi = (\partial V_\psi/\partial\psi)^{-1} \partial M_\psi/\rho \\ &= \partial M_\psi / \langle g^{-1} \rangle S_\psi \rho . \end{aligned} \tag{7}$$

Equation (7) can be combined with the general form of the equation of hydrostatic equilibrium,

$$\partial P/\partial\psi = -\rho , \tag{8}$$

to give

$$\frac{\partial P}{\partial M_\psi} = -\frac{G M_\psi}{4\pi r_\psi^4} f_p , \tag{9}$$

where

$$f_p = \frac{4\pi r_\psi^4}{GM_\psi S_\psi} \frac{1}{\langle g^{-1} \rangle} . \quad (10)$$

Because equation (1) preserves the spherical relationship between radius and volume, the energy conservation equation retains its nonrotating form; i.e.,

$$\frac{\partial L_\psi}{\partial M_\psi} = \epsilon - \frac{\partial E}{\partial t} - P \frac{\partial (1/\rho)}{\partial t} , \quad (11)$$

where L_ψ is the rate of energy flow past the surface ψ = constant, ϵ is the (nuclear-neutrino) energy generation rate per unit mass, E is the internal energy per unit mass, and t is time. The local flux of energy transported by radiation is

$$F = -\frac{4acT^3}{3\kappa\rho} \frac{\partial T}{\partial n} = -\frac{4acT^3}{3\kappa\rho} g \frac{\partial T}{\partial \psi} , \quad (12)$$

where a, c, and κ have their usual meanings. Using equation (7) in equation (12) gives

$$F = -\frac{4acT^3}{3\kappa} \langle g^{-1} \rangle S_\psi g \frac{\partial T}{\partial M_\psi} . \quad (13)$$

Integrating the flux over an equipotential surface gives, with equation (2),

$$L_\psi = -\frac{4acT^3}{3\kappa} \langle g^{-1} \rangle S_\psi^2 \langle g \rangle \frac{\partial T}{\partial M_\psi} . \quad (14)$$

Using equation (9), we rewrite equation (14) as

$$\frac{\partial \ln T}{\partial \ln P} = \frac{3\kappa}{16\pi acG} \frac{P}{T^4} \frac{L_\psi}{M_\psi} \frac{f_T}{f_p} , \quad (15)$$

where

$$f_T = \left(\frac{4\pi r_\psi^2}{S_\psi} \right)^2 \frac{1}{\langle g \rangle \langle g^{-1} \rangle} . \quad (16)$$

In the present formulation, we neglect the fourth effect of rotation on the equations (see above) and use the Schwarzschild criterion for convection. Then

$$\frac{\partial \ln T}{\partial \ln P} = \min \left[\nabla_{\rm ad}, \nabla_{\rm rad} \frac{f_T}{f_p} \right] , \quad (17)$$

where $\nabla_{\rm ad}$ and $\nabla_{\rm rad}$ are the normal (spherical) adiabatic and radiative gradients. We note that equation (11) is an approximation in that expansion and contraction will not, in general, maintain a conservative potential (cf. Kippenhahn and Möllenhoff 1974). As a result, the last two terms in equation (11) will not be constant over an equipotential surface. We assume that this effect will be compensated by large-scale circulation currents. Aside from this approximation and the neglect of the direct effect of rotation on convection, no other approximations have been made in transforming the spherical equations to equations with rotation.

Before describing the evaluation of the potential, a few comments on the above equations are in order. The first three effects of rotation, described at the beginning of this section, are contained in: the factor f_p, the interpretation of r_ψ through equation (1), and the evaluation of S_ψ and V_ψ, and the factor f_T, respectively. As the rate of rotation goes to zero, $f_p \to 1$, $f_T \to 1$, and $r_\psi \to r$, so the equations reduce to their spherical counterparts. The ratio f_T/f_p enters into the radiative equilibrium equation because we evaluate $\partial \ln T/\partial \ln P = (\partial \ln T/\partial M_\psi)/(\partial \ln P/\partial M_\psi)$, rather than $\partial \ln T/\partial M_\psi$. The approximation used by KMT and by Meyer-Hofmeister (1972) is *roughly* equivalent to considering only the factor f_p in equation (9). In general, f_p deviates from unity by a much larger amount than does f_T, so this would appear to be a consistent level of approximation. However, the ratio $f_T/f_p \sim 1/f_p$, which must appear in the criterion for convection (see eq. [17]), deviates from unity by an amount comparable to the deviation of f_p, and this should be taken into account at the level of approximation used by KMT and Meyer-Hofmeister.

A detailed description of the evaluation of the potential and the factors f_p and f_T is given in the Appendices. Basically, the potential is divided into three parts: ψ_s, the spherically symmetric part of the gravitational potential, ψ_r, the cylindrically symmetric potential directly due to rotation, and ψ_d, the cylindrically symmetric part of the gravitational potential due to distortion of the figure of the star. The evaluation of the first two parts is trivial. The third part is evaluated, at a given point, as if that point were on the surface of a polytrope rotating with constant ω and with the same ratio of mean interior density to central density as displayed by the model at the point in question. The distortion of the mass exterior to the equipotential surface which contains the point is ignored. As we will show in § III, this provides a very good approximation to the actual potential.

Equations (5), (9), (11), and (17) are similar enough to the spherical equations that they can easily be incorporated into existing stellar evolution codes. In our case, we have used the Paczynski code with modifications to the input physics as described by Endal (1975).

III. COMPARISON TO OTHER METHODS AND NUMERICAL TESTS

Several different methods have been used in the past to investigate the effects of rotation. Before describing the numerical tests of our program, we will discuss the similarities and differences among the various methods. We will not include perturbation techniques such as those of Chandrasekhar (1933) and Sweet and Roy (1953), which have been applied only to polytropes or other highly simplified stellar models.

a) Double-Approximation Method

This method has been used by a number of investigators (Roxburgh, Griffith, and Sweet 1965; Faulkner,

Roxburgh, and Strittmatter 1968; Strittmatter, Robertson, and Faulkner 1970; Sackmann and Anand 1970; Sackmann 1970), each of whom has introduced minor modifications. The method consists of dividing the star into two parts: a core which is assumed to be rotating slowly in comparison to the local critical velocity, and an envelope which contains a negligible amount of mass. First-order expansions in a rotation parameter are used in the core, and the Laplace equation is used for the potential in the envelope (the mass of the envelope does not contribute to the potential). For uniform rotation this is a valid approximation, but for differential rotation (rapidly rotating cores) the core approximation breaks down.

b) J^2 Method

A detailed description of the J^2 method has been given by Papaloizou and Whelan (1973). It has also been used by Whelan, Papaloizou, and Smith (1971), Whelan (1972), and Moss (1973). The stellar structure equations used in the J^2 method are formally equivalent to those used in the KT method, so the only difference is in the evaluation of the total potential, ψ. In the J^2 method, the Roche approximation has generally been used. This is equivalent to neglecting the contribution of the quantity ψ_d discussed in § II. The Roche approximation should break down in regions where the ratio of mean interior density to central density ($\langle\rho\rangle/\rho_c$) and the ratio of angular velocity to critical angular velocity (ω/ω_{cr}) are both significant compared with unity. This will be the case for rapid differential rotation in the core.

c) SCF Method

The self-consistent-field (SCF) method, as described by Ostriker and Mark (1968), is primarily a method for obtaining accurate solutions of the total potential and hydrostatic equilibrium equations. The SCF method was combined with the complete stellar structure equations by Jackson (1970; see also Mark 1968). Jackson's method was applied to differentially rotating stars on the upper main sequence by Bodenheimer (1971). In this method the stellar structure equations are evaluated on equipotential surfaces, as in the KT and J^2 methods. The primary difference is that the potential equation is solved much more accurately and the method is, as a result, very time-consuming. This makes it unsuitable for evolutionary calculations, but it remains a very powerful method for testing more approximate techniques.

Papaloizou and Whelan (1973) have made extensive comparisons of the results obtained with the various methods (including the KT method) for uniformly rotating ZAMS models. Except at low masses ($M \leq 1\ M_\odot$), they find that all the methods described above produce essentially the same results. At low masses the comparisons seem to be complicated by differences in the methods used for handling convective envelopes (see Aranda and Thomas 1975). Since we will not be computing models of low-mass stars, we will not worry about this problem. Above 1 $M_\odot$, the reduction in the luminosity produced by uniform rotation is confined to <10 percent, and this reduction varies linearly with ω^2. This indicates that uniform rotation may be considered as a small perturbation on nonrotating models and, therefore, does not constitute a very stringent test for methods which will be used when rotation introduces large changes in the models. Unfortunately, there are very few calculations with which we can compare our results for differentially rotating models.

Bodenheimer (1971) has calculated ZAMS models of 15, 30, and 60 $M_\odot$ stars with strong differential rotation using the SCF method. In the models computed by Bodenheimer, the velocity was constant on cylinders, whereas we have specified constant angular velocities on equipotential surfaces, so the results obtained by the two methods may not be directly comparable. However, Bodenheimer found that, to a good approximation, the effects of rotation on the central temperature T_c, central density ρ_c, and luminosity L do not depend on the distribution of angular momentum but only on the total angular momentum J of the models. If we confine ourselves to these parameters, the comparison *may* be valid. Figure 1 shows the variations of these parameters, for a 30 $M_\odot$ star, as a function of log J. The SCF results are indicated by the symbols used in Figure 5 of Bodenheimer. The different symbols refer to different internal distributions of the angular momentum. The results obtained with our method are indicated by dashed lines. We have specified that ω/ω_{cr} (at the equator) be constant throughout our models. The values of ω/ω_{cr} at various values of log J are indicated at the top of the figure. Up to $\omega/\omega_{cr} = 0.8$, the differences between our models and the SCF models with the same value of J are generally comparable to the scatter introduced by different angular momentum distributions in the SCF models. Beyond $\omega/\omega_{cr} = 0.8$, we were not able to produce converged models because of the large differences between the (nonrotating) Schwarzschild model used as an initial guess and the rotating models to be calculated by relaxation. We should emphasize here that the convergence problem is due to a poor initial guess, rather than to limitations of our method. In the evolutionary sequences presented in § V, ω/ω_{cr} was as large as 0.99. In these calculations, there were no problems with convergence because the initial guesses were based on extrapolations of models which were already rapidly rotating.

IV. THE EVOLUTION OF A 7 $M_\odot$ STAR: STARTING MODELS AND ROTATION LAWS

In order to explore the effects of rotation on the post–MS stages of evolution, five sequences of models were computed for a 7 $M_\odot$ star; one sequence for a nonrotating star (case 0), and four sequences for rotating stars with different assumptions about the redistribution of angular momentum in an evolving star (cases 1–4). For each case, the sequence was begun on the ZAMS with a chemical composition of $X = 0.7$, $Z = 0.03$. The prescriptions for $\omega(M_\psi)$ used in the various cases are summarized in Table 1.

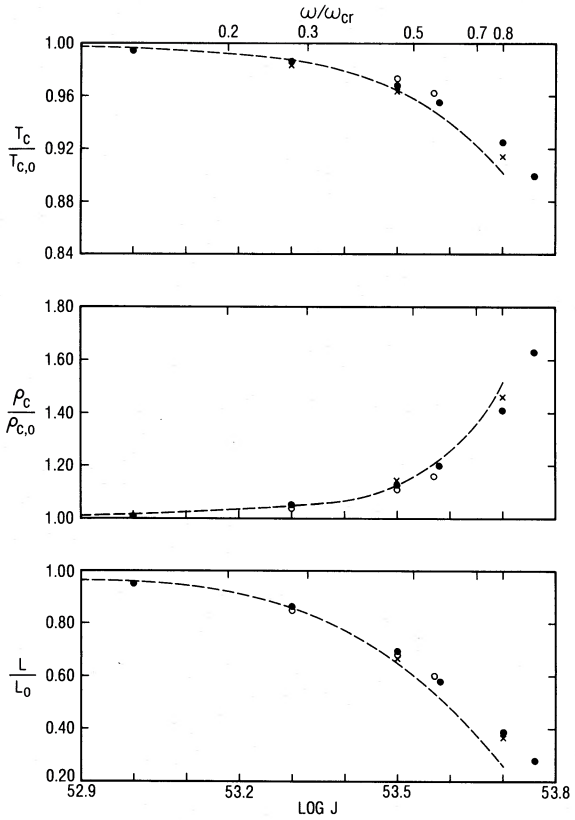

FIG. 1.—The effects of differential rotation on a 30 $M_\odot$ ZAMS model as predicted by the KT method (*dashed line*) and by the SCF calculations of Bodenheimer (1971, *symbols*). The zero subscript refers to the nonrotating model, which is compared with rotating models with different values of the total angular momentum J. For the KT models, the angular velocity distribution was spherical with constant ω/ω_{cr} (in the equatorial plane) throughout the star. Values of ω/ω_{cr} are given at the top. For the SCF models, the different symbols refer to different angular velocity distributions and are the same as used in Fig. 5 of Bodenheimer (1971).

In all cases, the angular momentum was assumed to be constant on equipotential surfaces, instead of on cylinders, as in the models of Bodenheimer (1971). This has already been discussed in § III and will be discussed further in § VI. Also, in conserving angular momentum, deformation of the equipotential surfaces was ignored; i.e., the moment of inertia of a given mass shell was assumed to be that of a thin spherical shell of radius r_ψ. Cases 1–3 were begun with solid-body rotation and $\omega = 8.8 \times 10^{-5}\ s^{-1}$. This corresponds to the average rotation rate for spectral type B5 main-sequence stars, according to Abt and Hunter (1962). Unlike the models computed by KMT and Meyer-Hofmeister, our models are not rapid rotators on the MS. The case 4 sequence was begun with solid-body rotation at $\omega = 8.8 \times 10^{-5}\ s^{-1}$ in the regions outside the convective core. Within the convective core, we set $\omega = \min\ [8.8 \times 10^{-5}\ s^{-1}\ (r_{cc}/r)^2,\ 0.9\ \omega_{cr}]$, where r_{cc} is the radius of the convective core. Limiting ω to 90 percent of ω_{cr} was necessary to avoid the supercritical velocities near the center implied by the $\omega r^2 =$ constant prescription. This limit on ω was also applied to the convective regions of the evolving models for case 4. The extra angular momentum was uniformly redistributed throughout the remainder of the convective region whenever the limiting velocity was reached.

The rotation laws chosen are not meant to accurately reflect the effects of the various angular momentum redistribution mechanisms which may operate in an evolving star. Rather, they are meant to bracket the set of physically plausible rotation laws. Cases 1 and 3 represent extremes in terms of complete redistribution of angular momentum and no redistribution of angular momentum, respectively. Case 2 represents an intermediate (and more likely) possibility that, while circulation currents redistribute the angular momentum in chemically homogeneous radiative regions, such currents are choked off in inhomogeneous regions by gradients in the mean molecular weight (cf. Mestel 1953). In convective regions, the high viscosity associated with turbulence may lead to solid-body rotation. Case 4 represents an alternate possibility, namely, that mass motions in convective regions tend to equalize the specific angular momentum in such regions. This would be the case if the circulation produced by convection preserves the angular momentum of the convective elements and has, to some extent, been borne out by calculations (Tayler 1973; Weir 1975). Some justification for limiting the angular velocity to some fraction of the critical velocity is also provided by these calculations, though the choice of 0.9 ω_{cr} for the limiting angular velocity is entirely arbitrary. Actually, constant specific angular momentum implies that

TABLE 1*

PRESCRIPTIONS FOR $\omega(M_\psi)$

REGION	CASE				
	0	1	2	3	4
Radiative and chemically homogeneous.....	...	...	SB	...	SB
Radiative and chemically inhomogeneous.....	$\omega = 0$ (nonrotating)	SB	LC	LC	LC
Convective.....	...	...	SB	...	CA

* ABBREVIATIONS: SB, solid body rotation and overall conservation of angular momentum. LC, local conservation of angular momentum, CA — $\omega r^2 =$ constant (but $\omega \leq 0.9\ \omega_{cr}$) and overall conservation of angular momentum (see text).

TABLE 2

EVOLUTION TIME SCALES*

Stage	Symbol	Case 0	Case 2	Case 3	Case 4
ZAMS	A	0.0	0.0	0.0	0.0
H exhaustion	B	32.861	33.208	33.676	33.706
	$\tau(A \rightarrow B)$	32.861	33.208	33.676	33.706
	τ/τ_0	...	1.011	1.025	1.026
He ignition	C	35.392	35.803	36.311	36.475
	$\tau(B \rightarrow C)$	2.531	2.594	2.635	2.769
	τ/τ_0	...	1.025	1.041	1.094
He exhaustion	D	50.806	51.691	52.233	55.049
	$\tau(C \rightarrow D)$	15.415	15.888	15.922	18.573
	τ/τ_0	..	1.031	1.033	1.205
Envelope intrusion	E	51.767	52.842	53.506	...
	$\tau(D \rightarrow E)$	0.961	1.151	1.273	...
	τ/τ_0	...	1.198	1.325	...
H reignition	F	51.870	52.962	53.645	...
	$\tau(E \rightarrow F)$	0.103	0.120	0.139	...
	τ/τ_0	...	1.165	1.350	...

* Time scales are in units of 10^6 years.

$\omega\bar{\omega}^2$ = constant, where $\bar{\omega}$ is the distance from the rotation axis. However, within the restriction that ω be constant on spherical surfaces ωr^2 = constant is the closest possible approximation.

V. THE EVOLUTION OF A 7 $M_\odot$ STAR: RESULTS

The case 1 sequence was terminated during helium burning in the core. At this point it was clear that the effects of rotation on the post–MS evolution are negligible if solid-body rotation throughout the star is maintained during these stages. Unless coupling mechanisms, such as magnetic fields, which do not directly depend on circulation currents are stronger than one would normally expect, solid-body rotation throughout the star will probably not be maintained. In any case, the numerous previous calculations for nonrotating stars adequately describe the case 1 evolution, so case 1 will not be discussed further. Cases 2–4 were continued until critical velocities were encountered at some point in the star. In all three cases, this occurred after helium exhaustion in the core and prior to carbon ignition.

a) Time Scales

One of the effects of rotation is to lengthen the time scales for the evolution. Table 2 gives the ages of the models at a number of stages for case 0 and cases 2–4. Hydrogen and helium exhaustion are defined to occur when the abundances of the respective nuclei drop below the minimum abundance (10^{-4}) allowed for in the code. Helium ignition is defined to occur at the first appearance of a convective core due to helium burning. Some helium burning, as evidenced by a slight decrease in the helium abundance, generally occurs before this, but the first appearance of a convective core provides a convenient point at which to compare the models in the various sequences. Subsequent to helium exhaustion, the hydrogen-burning shell is extinguished and the convective envelope intrudes into the hydrogen-exhausted core, reducing the size of the core. This stage, and the stage at which the maximum depth of the convective envelope is reached and the hydrogen-burning shell reignited, were chosen as two more points at which to compare the sequences. Below the ages at each stage, the times required to evolve from the previous stage are given. Finally, for cases 2–4, this time is compared with the time required by the nonrotating (case 0) models. In case 4, critical velocities were reached prior to the envelope intrusion stage. Inspection of Table 2 shows that the time scales for the evolution are not grossly affected by rotation. Except for case 4, the increases in the time scales prior to helium exhaustion are less than 5 percent. The 20 percent increase in the duration of helium burning in case 4 is larger than the present uncertainty in the time scales for nonrotating models, but it is also strongly dependent on the limiting angular velocity allowed in the convective core.

b) Loops in the H-R Diagram

Figure 2 shows the tracks of the sequences for cases 2–4 in the H-R diagram. The points at which the stages listed in Table 2 occur are indicated by the letter symbols given in Table 2. For comparison, the case 0 track is shown with dashed lines. Here again, the effects of rotation are strongest for case 4. There appear to be three loops for this case, but the first (shortest) loop may be due to a problem in locating the outer boundary of the convective core (cf. Paczynski 1970, for a discussion of this problem). We later recalculated the evolution through these stages (for case 4 only) using shorter time steps and a finer criterion for the size of the convective core. In this calculation, the first and second loops merged into a single loop resembling the loop for case 0, though extending to slightly higher effective temperatures. However, the loop which occurs during the helium-shell-burning phase (containing point D) still appeared, indicating that it is real and that multiple loops can result from rotation. We show the track for

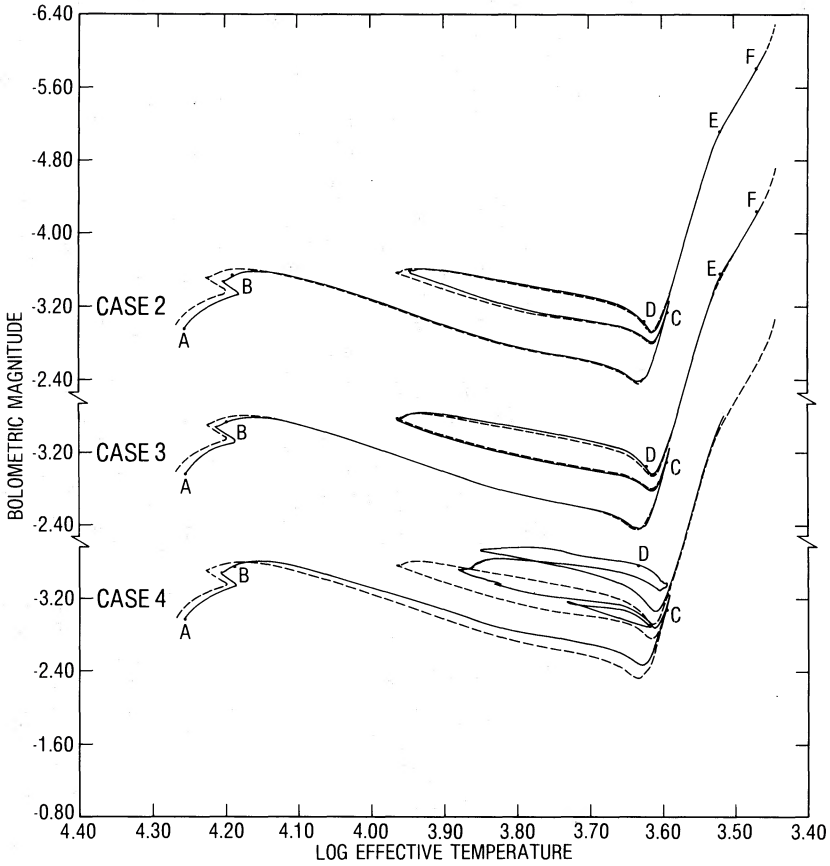

FIG. 2.—The H-R diagrams for cases 2–4. The stages referred to in Table 2 are indicated by capital letters. The case 0 track is indicated by dashed lines.

our first calculation because that is the sequence which was continued into the post-loop stages. The later calculation was discontinued once it was confirmed that the changes in the loops do not affect the post-loop evolution.

The results of KMT and Meyer-Hofmeister have already indicated that rotation can increase the size and number of loops. However, while they began their models with critical velocities on the ZAMS, we begin ours with more typical velocities ($\sim\frac{1}{2}$ critical). Our cases 2 and 3, which differ from KMT and Meyer-Hofmeister primarily in the initial velocities, show no gross effects in the H-R diagram due to rotation. These effects depend critically on the assumed initial velocity.

Only a small percentage of stars begin their evolution with near critical velocities. Moreover, Kraft (1966) has shown that the observed rotational velocities of Cepheids indicate the loss of a considerable fraction of the MS angular momentum. Consequently, the interpretation by Meyer-Hofmeister that rotation affects the statistics of Cepheids by shifting downward in mass the peak in the number versus mass distribution is questionable.

One further comment should be made about Figure 2. At point E, the giant branches of our sequences show a pronounced bending to the right. This is the point at which intrusion of the convective envelope into the hydrogen-exhausted core begins. This mixes material from the core into the envelope and lowers the hydrogen abundance there. To take this into account in the envelopes, the opacities from the tables (which applied to the ZAMS composition) were reduced as if the opacity were due to pure electron scattering in an ionized medium. Since much of the mass in the envelopes during this stage lies above the hydrogen ionization zone, the effect of the reduction of the hydrogen abundance in the envelope was overestimated by this method.

c) *Conditions at the Center*

Figure 3 shows the paths of the sequences for cases 2–4 in the (log central density, log central temperature)-plane. Again, the stages referred to in Table 2 are indicated by capital letters, and the case 0 sequence is shown by dashed lines. Figures 4–6 show the angular velocities (*solid lines*) of the innermost mass zone as functions of the model numbers. The dashed lines show ω/ω_{cr} for the same zone. The letters at the tops of the figures refer to the evolutionary stages. The discontinuous nature of the angular velocity curves

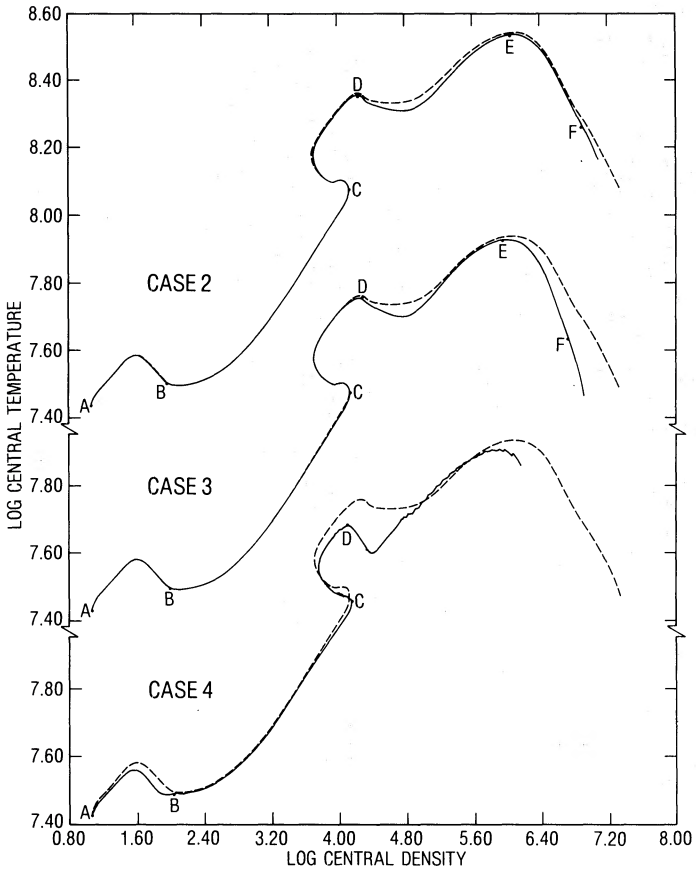

FIG. 3.—The paths in the (log ρ_c, log T_c)-plane for cases 2–4. Stages are indicated by capital letters. The trajectory of the case 0 sequence is indicated by dashed lines.

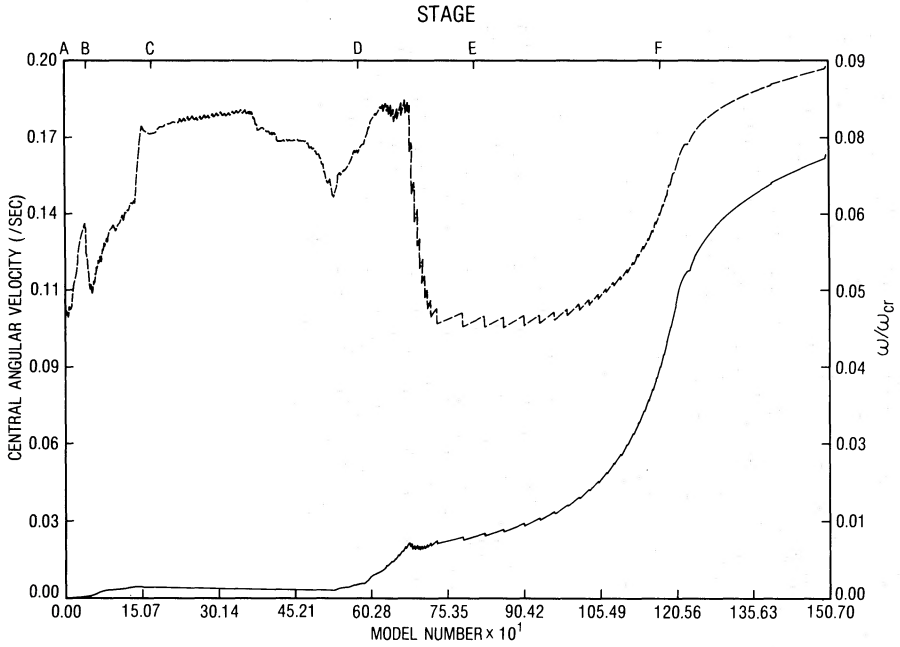

FIG. 4.—The angular velocity at the innermost mass zone as a function of MODEL NUMBER for case 2. The angular velocity in the equatorial plane is shown by a solid line and ω/ω_{cr} by a dashed line. The numbers are rounded to two decimal places.

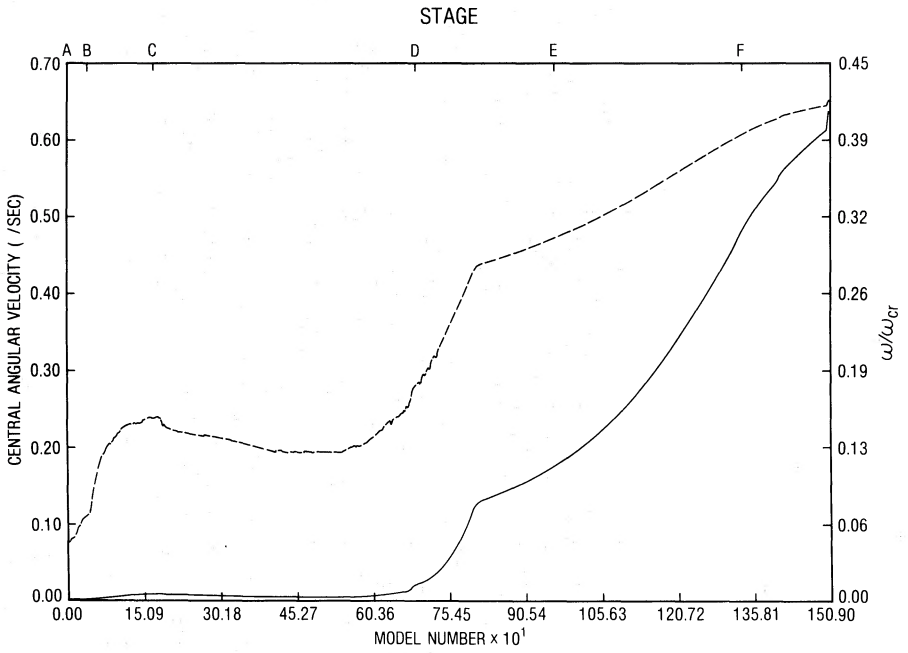

FIG. 5.—Same as Fig. 4, but for case 3

for cases 2 and 4 is due to the finite zoning of the models. For instance, after helium exhaustion (point D), the helium-exhausted core grows by finite increments as the helium-burning shell moves outward. Whenever the helium abundance in a shell reaches zero and that shell becomes part of the core (which is rotating as a solid body), the shell's angular momentum and moment of inertia are included in computing the angular velocity of the core in the next model. This causes a sudden drop in the core angular velocity.

From Figure 3, it is apparent that, for cases 2 and 3, rotation does not significantly affect the central conditions until after helium exhaustion (point D). For case 4, however, there are noticeable effects during both the hydrogen- and helium-burning stages. Figure 6 shows that the angular velocity of the inner shell is at the limiting velocity during these stages, and therefore the magnitudes of these effects depend on the chosen limiting velocity. After convection in the core dies out and before the fuel is completely exhausted,

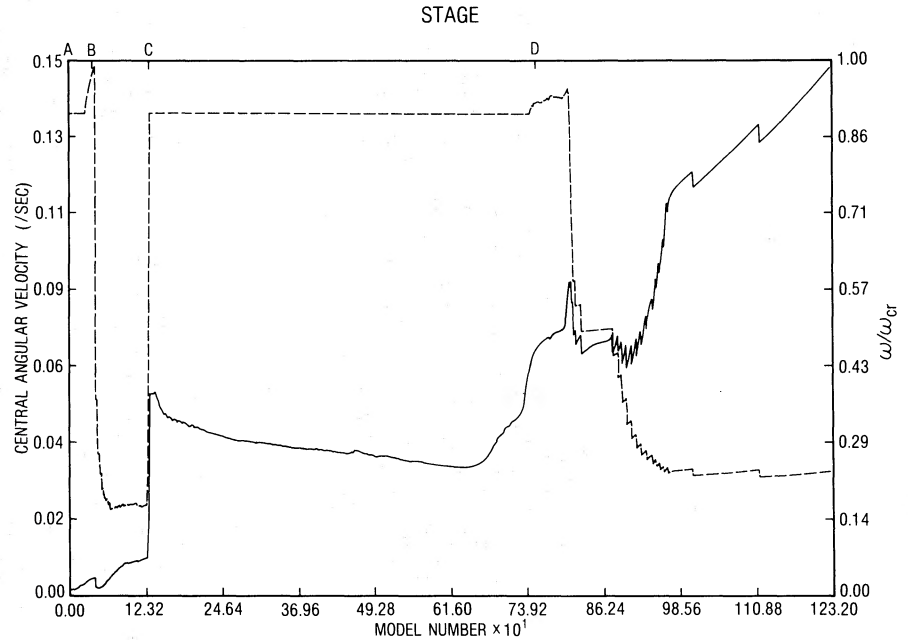

FIG. 6.—Same as Fig. 4, but for case 4

there is a short period when the core rotates with local conservation of angular momentum and with no limiting velocity. After the hydrogen-burning stage, the angular velocity reaches 99 percent of ω_{cr}, during this period.

After helium burning, rotation becomes more and more important in all cases as the core contracts and the angular velocity increases rapidly. In general, rotation causes the temperature, at a given density, to be lower in the rotating models than in the nonrotating models. Thus, carbon ignition will become very difficult to achieve unless some mechanism couples the core to the envelope. In view of the large gradient in the mean molecular weight across the hydrogen-burning shell, it is difficult to see how this coupling will occur. (However, KMT have suggested some possible mechanisms.)

d) The Evolution of the Angular Velocity Distribution

After hydrogen burning, the contractions and expansions of various parts of the star plus the assumed rotation laws produce strong differential rotation. This is illustrated in Figures 7–9, which show the angular velocities and ω/ω_{cr} as functions of the mass coordinate for cases 2–4, respectively. Each figure shows models at stages A, C, and D and a model close to the end of the sequence. A general feature of all the cases is the spin-up of the core. Critical velocities were reached in each case soon after the last model shown in the figures. The critical velocities were reached not at the center, but instead at the outer edge of the hydrogen-exhausted (case 3) or helium-exhausted (cases 2 and 4) core. This situation can be seen, for cases 2 and 4, as a direct result of imposing solid-body rotation in the chemically homogeneous core. For case 3, the occurrence of critical velocities at the outer edge of the core can be understood by considering the structure of a nearly isothermal, degenerate core. For a nonrelativistic, degenerate core, the density distribution is very similar to that of a $n = 1.5$ polytrope (Chandrasekhar 1939). The density distribution in the convective core of the ZAMS model can also be approximated by an $n = 1.5$ polytrope. For local conservation of angular momentum, the evolution of the angular velocity distribution is determined by the evolution of the density distribution. Thus the angular velocity distribution in the degenerate core of the final model is very similar to that of the ZAMS model, i.e., flat, though the value of the angular velocity in the final model is almost four orders of magnitude larger. This nearly flat distribution causes ω/ω_{cr} to increase outward from the center.

In all of our rotation laws, we have ignored the possibility that instabilities can overcome gradients in the mean molecular weight (μ-barriers). However, for large enough gradients in the angular velocity and small enough gradients in the mean molecular weight,

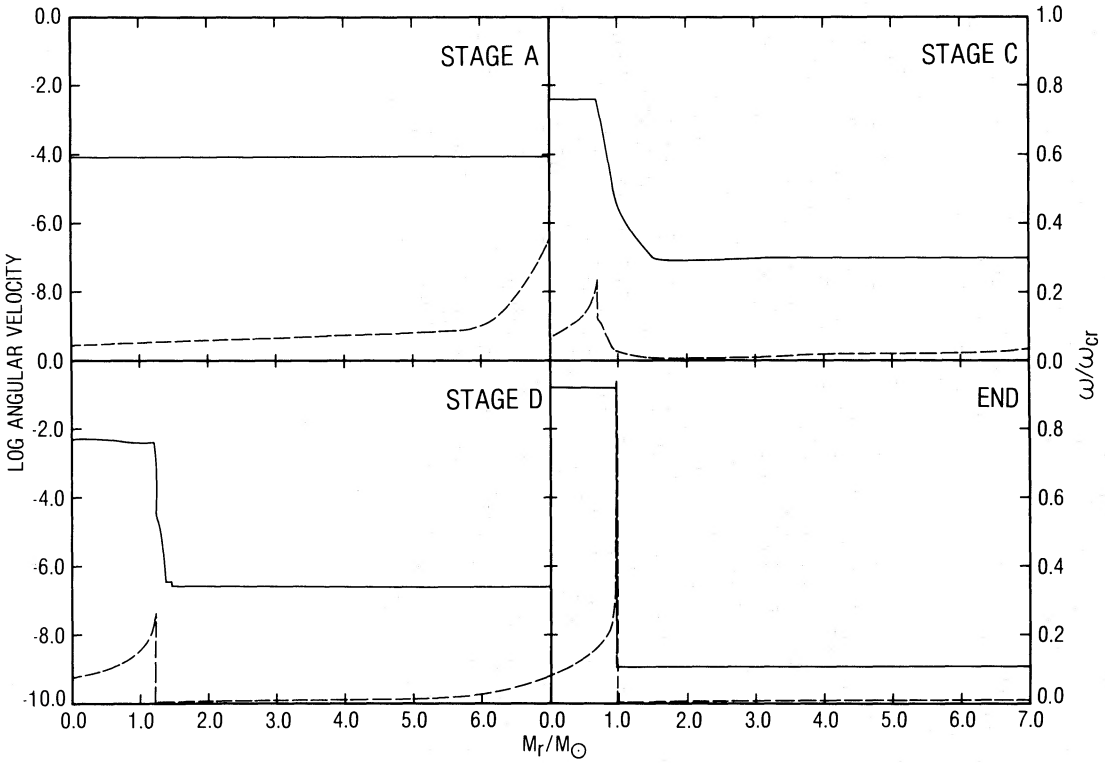

FIG. 7.—The angular velocity distribution throughout the models at four stages in the case 2 sequence. The angular velocities are indicated by solid lines; ω/ω_{cr}, by dashed lines.

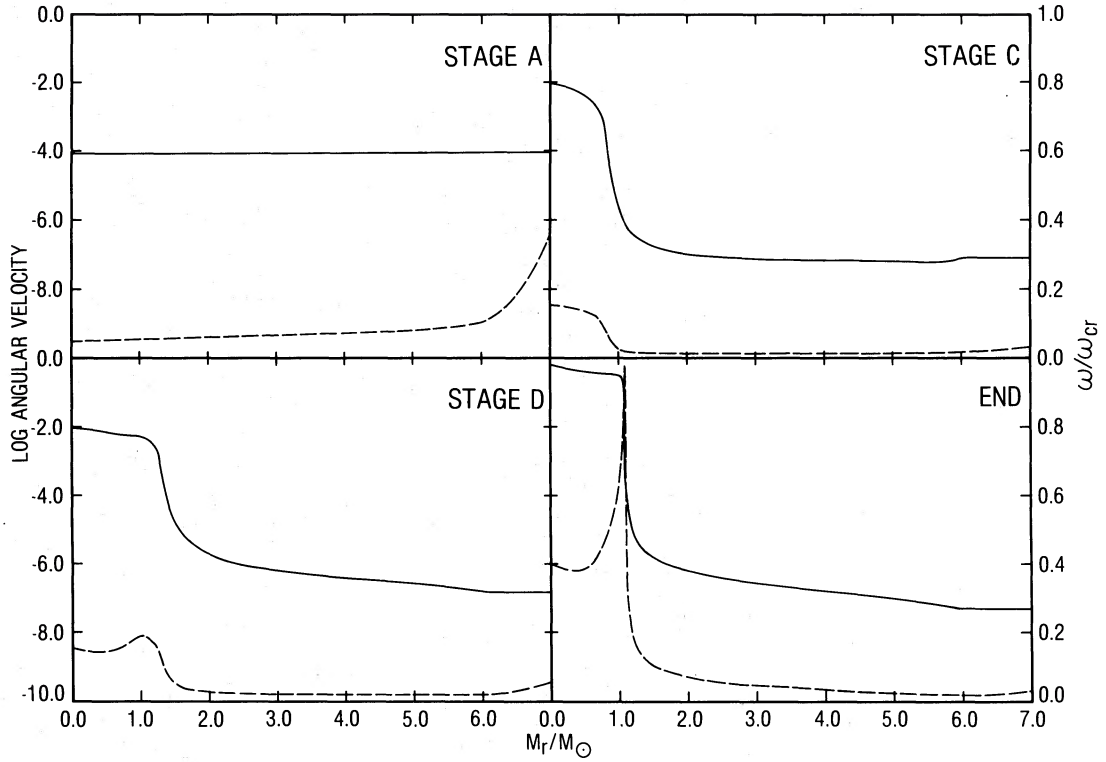

FIG. 8.—Same as Fig. 7, but for case 3

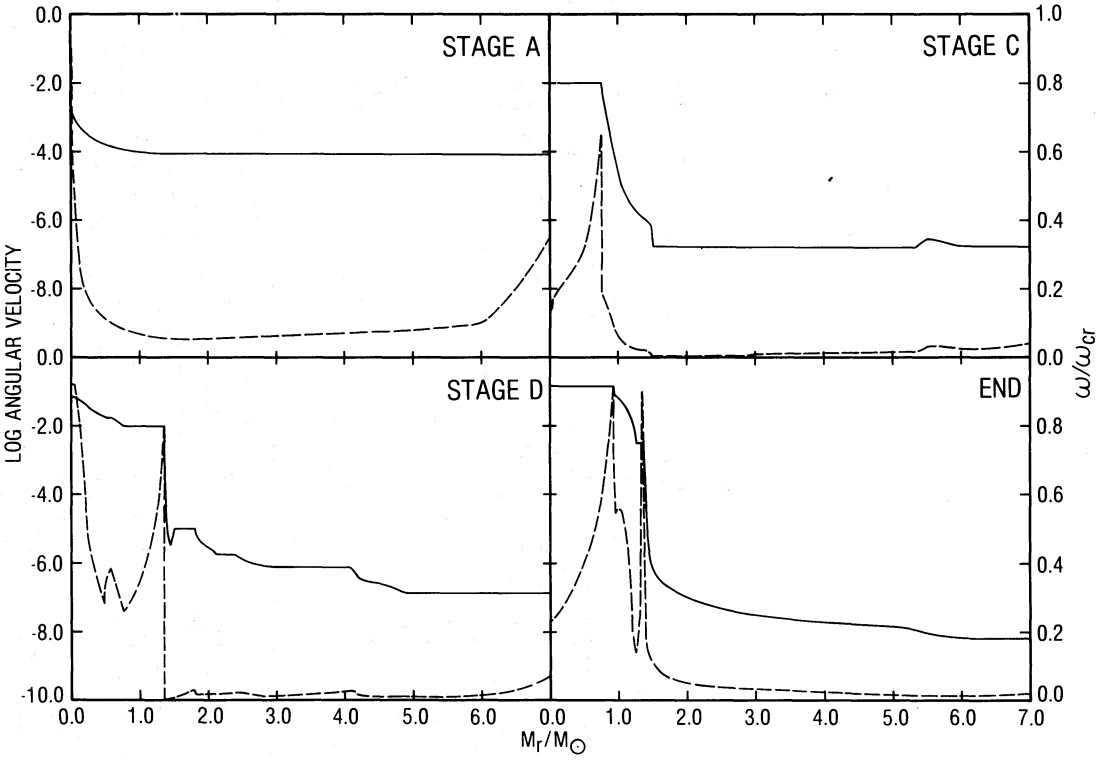

FIG. 9.—Same as Fig. 8, but for case 4

instabilities can occur (cf. Zahn 1974). In the region of transition from the carbon-oxygen core to the helium-rich zone, the gradient in the mean molecular weight is fairly small and, in cases 2 and 4, the gradients in the angular velocity are very large. If we had included such instabilities, redistribution of the chemical composition, as well as the angular momentum, would have occurred. The effect this would have on the models is difficult to predict without detailed calculations, since the effect would depend on the interaction of several factors: the degree of mixing produced by the instability, the effect of the mixing on the helium-burning shell, the time scale for reestablishing something like solid-body rotation in the core, etc.

VI. DISCUSSION AND CONCLUSIONS

The formulation we have used for the stellar structure equations assumes that the total potential is conservative. Our rotation laws (constant ω on equipotential surfaces) are not conservative, except in regions with solid-body rotation. The result of such nonconservative rotation laws will be that ρ and T are not strictly constant on equipotential surfaces. Although we have not explored in detail the effects this would have on the models, we may hope that any such effects will be smoothed by circulation currents which generally operate very efficiently along equipotentials. The numerical tests presented in § III indicate that our models agree well with models employing conservative potentials.

The results presented in § V extend to stars with typical rotation velocities several features already known from computations of rapidly rotating stars. These features include the small effect of rotation on the total time scale of evolution and the development of critical velocities in the core. These conclusions could have been arrived at by simply scaling down the results for rapid rotators, so they do not constitute new results. One somewhat surprising feature, however, is that rather large initial rotation velocities (or extreme angular momentum distributions) are needed to affect the loops in the H-R diagram significantly.

Although our results indicate that the effects of rotation are small prior to core helium exhaustion, the situation is very different for the subsequent stages. Once the rotation velocities in the core reach near-critical values, the star has two choices. The first choice, which can only be a temporary solution, is to stop the core contraction and thus avoid critical velocities. The second, and inevitable, solution is to transfer angular momentum from the core to the envelope. It appears that secular instabilities such as the Goldreich-Schubert instability can, at least, overcome the weak μ-barrier at the outer edge of the carbon-oxygen core. This will redistribute angular momentum, but it will also mix helium into the core. How this mixing will affect the subsequent evolution cannot be determined without further calculations, but it is clear that the effects will be significant. Such calculations will be the subject of the next paper in this series.

APPENDIX A

APPROXIMATION FOR THE POTENTIAL AND EVALUATION OF THE FACTORS f_p AND f_T

We divide the total potential, ψ, into three parts, as discussed in § II. In view of the high degree of central condensation of stars, we assume that, at a point p on the surface ψ = constant, only the mass enclosed by that surface contributes to ψ_d. If the coordinates of the point p are radius r and polar angle θ, the components of the potential at p can be written as (cf. Kopal 1959):

$$\psi_s = \frac{GM_\psi}{r}, \tag{A1}$$

$$\psi_r = \tfrac{1}{2}\omega^2 r^2 \sin^2\theta, \tag{A2}$$

and

$$\psi_d = \sum_{j=2}^{\infty} \frac{4\pi G}{(2j+1)r^{j+1}} \int_0^{r_0} \rho \frac{\partial}{\partial r_0'}(r_0'^{j+3} Y_j) dr_0', \tag{A3}$$

where r_0 is the radius of the equipotential surface at the angle θ_0, defined such that $P_2(\cos\theta_0) = 0$, P_2 is the second-order Legendre polynomial, and Y_j is the axisymmetric tesseral harmonic relating r to r_0 on a given equipotential surface:

$$r(r_0, \theta) = r_0\left[1 + \sum_j Y_j(r_0, \theta)\right]. \tag{A4}$$

Consistent with the approximation for ψ_d mentioned above, Y_j is given by

$$Y_2 = -\frac{\omega^2 r_0^2}{3GM_\psi} \frac{5}{2 + \eta_2(r_0)} P_2(\cos\theta) \tag{A5a}$$

and

$$Y_j = 0 \quad \text{for} \quad j \neq 2, \tag{A5b}$$

where η_2 is the logarithmic derivative of Y_2 with respect to r_0:

$$\eta_2 = \frac{r_0}{Y_2}\frac{\partial Y_2}{\partial r_0}. \tag{A6}$$

This quantity can be evaluated by integration of Radau's equation (cf. Kopal 1959):

$$r\frac{d\eta_j}{dr} + 6\frac{\rho}{\langle\rho\rangle}(\eta_j + 1) + \eta_j(\eta_j - 1) = j(j+1) \tag{A7}$$

with $j = 2$ and the boundary condition $\eta_j(0) = j - 2$. Using equation (A6), we can evaluate the derivative in equation (A3) as follows:

$$\frac{\partial}{\partial r_0}(r_0^5 Y_2) = 5r_0^4 Y_2 + r_0^5\frac{\partial Y_2}{\partial r_0} = r_0^4 Y_2\left(5 + \frac{r_0}{Y_2}\frac{\partial Y_2}{\partial r_0}\right),$$

or

$$\frac{\partial}{\partial r_0}(r_0^5 Y_2) = r_0^4 Y_2(5 + \eta_2). \tag{A8}$$

At this point, we can write the total potential as

$$\psi = \frac{GM_\psi}{r} - \frac{4\pi}{3r^3}P_2(\cos\theta)\int_0^{r_0}\frac{\rho r_0'^6}{M_\psi}\omega^2\frac{5+\eta_2}{2+\eta_2}dr_0' + \tfrac{1}{2}\omega^2 r^2\sin^2\theta, \tag{A9}$$

where all the quantities within the integral are to be evaluated at the point referred to by the dummy-variable-of-integration.

If we define

$$A = \frac{\omega^2 r_0^2}{3GM_\psi}\frac{5}{2+\eta_2(r_0)}, \tag{A10}$$

then the equation of an equipotential surface is, from equations (A4) and (A5),

$$r = r_0[1 - AP_2(\cos\theta)]. \tag{A11}$$

In order to relate r_0 to r_ψ, we evaluate the volume integral from $r = 0$ to r given by equation (A11). This gives

$$V_\psi = \frac{4\pi}{3}r_0^3[1 + \tfrac{3}{5}A^2 - \tfrac{2}{35}A^3]; \tag{A12}$$

so, from equation (1),

$$r_\psi = r_0[1 + \tfrac{3}{5}A^2 - \tfrac{2}{35}A^3]^{1/3}. \tag{A13}$$

In practice, one knows r_ψ and wants to find r_0. Since A is a function of r_0, this must be done by an iterative procedure.

Since the local effective gravity is given by

$$g = \frac{\partial\psi}{\partial n} = \left[\left(\frac{\partial\psi}{dr}\right)^2 + \left(\frac{1}{r}\frac{\partial\psi}{\partial\theta}\right)^2\right]^{1/2}, \tag{A14}$$

g can be found by differentiation of equation (A9). The integral in equation (A9) and its derivatives must be evaluated numerically. Once g and g^{-1} are known for a set of points on an equipotential surface, $S_\psi\langle g\rangle$ and $S_\psi\langle g^{-1}\rangle$ can be found from equation (2) by numerically integrating over θ.

In the procedure we have used, η_2 is not evaluated by direct integration of equation (A7). Instead, the ratio $\langle\rho\rangle/\rho_c$ is evaluated at the point p and η_2 is assigned the value appropriate for the surface of a polytrope with the same value of $\langle\rho\rangle/\rho_c$. The values of η_2 (as a function of the polytropic index) were taken from Kopal (1959) and the values of $\langle\rho\rangle/\rho_c$ from Chandrasekhar (1939). Test models computed with direct integration of equation (A7) showed that this approximation has no discernible effect on the models. At this point, all the quantities needed in equations (10) and (16) to evaluate f_p and f_T are known.

APPENDIX B

IMPLEMENTATION IN THE STELLAR EVOLUTION CODE

I. ENVELOPES

The Paczynski code uses a separate program to calculate a grid of envelopes in the ($\log L$, $\log T_0$)-plane, where T_0 is the temperature of the outermost shell in the envelope (for a complete description of this program, see Paczynski 1969). These envelopes are then used to provide outer boundary conditions for the interior (Henyey) program. Because the envelopes are constructed before the interior structure is known, the integral in equation (A9) cannot be directly evaluated and the following approximation is used.

Let B denote the integral in equation (A9). We evaluate B, for the envelope only, as if the interior were a polytrope rotating as a solid body. Then ω and η_2 are constant and can be taken outside of the integral. For a polytrope of index n, $\rho/\rho_c = \theta^n$, where θ is the Lane-Emden function (not to be confused with the angle θ). If we introduce the variable $\xi = (r_0/R)\xi_1$ where R is the radius of the polytrope and ξ_1 is the first zero of the Lane-Emden function, then

$$B = \omega^2\left(\frac{R}{\xi_1}\right)^7 \frac{5+\eta_2}{2+\eta_2}\rho_c \int_0^{\xi} \frac{\theta^n \xi'^6}{M_{\xi'}} d\xi' . \tag{B1}$$

The interior mass in a polytrope obeys the equation

$$M_\xi = 4\pi\rho_c\left(\frac{R}{\xi_1}\right)^3\left(-\xi^2\frac{\partial\theta}{\partial\xi}\right), \tag{B2}$$

so

$$B = \frac{\omega^2}{4\pi}\left(\frac{R}{\xi_1}\right)^4 \frac{5+\eta_2}{2+\eta_2}\int_0^{\xi} \frac{\theta^n \xi'^4}{(-\partial\theta/\partial\xi')} d\xi' . \tag{B3}$$

Equating R with r_0 and rewriting the above equation as

$$\frac{B}{\omega^2 r_0^4} = -\frac{1}{4\pi}\frac{1}{\xi_1^4}\frac{5+\eta_2}{2+\eta_2}\int_0^{\xi_1} \frac{\theta^n \xi'^4}{(-\partial\theta/\partial\xi')} d\xi' \tag{B4}$$

yields an equation which contains only quantities related to polytropes on the right-hand side. The solutions of the Lane-Emden equation given by Comrie (1932) were used to evaluate equation (B4) for $n = 1.5, 2, 2.5, \ldots, 5$, and the results put into the envelope program as a table. The same procedure for interpolation in $\langle\rho\rangle/\rho_c$ as used for finding η_2 (see Appendix A)is then used to find $B/\omega^2 r_0^4$.

This procedure requires that ω and ρ_c be known beforehand. It is assumed that ω is constant throughout the envelope, and the two-dimensional grid of envelopes is replaced by a four-dimensional grid in ($\log L$, $\log T_0$, ω, ρ_c). In practice, the envelope program is used as a subroutine of the Henyey program which calls for new envelopes whenever the models run out of the old grid. In this way, the grids can be kept small without frequently having to stop the run to calculate new envelopes.

II. INTERIORS

For the interior (Henyey) part of the calculation, the equations in Appendix A are used, with no further approximations.

REFERENCES

Abt, H. A., and Hunter, J. H., Jr. 1962, *Ap. J.*, **136**, 381.
Aranda, J., and Thomas, H.-C. 1975, *Astr. and Ap.*, **45**, 441.
Bodenheimer, P. 1971, *Ap. J.*, **167**, 153.
Chandrasekhar, S. 1933, *M.N.R.A.S.*, **93**, 390.
———. 1939, *An Introduction to Stellar Structure* (Chicago: University of Chicago Press).
Comrie, L. J. 1932, *Mathematical Tables, British Association for the Advancement of Science*, Vol. **2** (London: Office of the British Association).
Cowling, T. G. 1951, *Ap. J.*, **114**, 272.
Endal, A. S. 1975, *Ap. J.*, **195**, 187.
Faulkner, J., Roxburgh, I. W., and Strittmatter, P. A. 1968, *Ap. J.*, **152**, 203.
Jackson, S. 1970, *Ap. J.*, **161**, 579.
Kippenhahn, R., Meyer-Hofmeister, E., and Thomas, H.-C. 1969, *Astr. and Ap.*, **5**, 155 (KMT).
Kippenhahn, R., and Möllenhoff, C. 1974, *Ap. and Space Sci.*, **31**, 117.
Kippenhahn, R., and Thomas, H.-C. 1970, in *Stellar Rotation*, ed. A. Slettebak (Dordrecht: Reidel), p. 20 (KT).
Kopal, Z. 1959, *Close Binary Systems* (New York: Wiley).
Kraft, R. P. 1966, *Ap. J.*, **144**, 1008.
Maeder, A. 1974, *Astr. and Ap.*, **34**, 409.
Mark, J. 1968, *Ap. J.*, **154**, 627.
Mestel, L. 1953, *M.N.R.A.S.*, **113**, 716.
Meyer-Hofmeister, E. 1972, *Astr. and Ap.*, **16**, 282.
Moss, D. L. 1973, *M.N.R.A.S.*, **161**, 225.
Ostriker, J. P., and Mark, J. 1968, *Ap. J.*, **151**, 1075.
Paczynski, B. 1969, *Acta Astr.*, **19**, 1.
———. 1970, *Acta Astr.*, **20**, 195.
Papaloizou, J. C. B., and Whelan, J. A. J. 1973, *M.N.R.A.S.*, **164**, 1.

Randers, G. 1942, *Ap. J.*, **95**, 454.
Roxburgh, I. W., Griffith, J. S., and Sweet, P. A. 1965, *Zs. f. Ap.*, **61**, 203.
Sackmann, I.-J. 1970, *Astr. and Ap.*, **8**, 76.
Sackmann, I.-J., and Anand, S. P. S. 1970, *Ap. J.*, **162**, 105.
Sackmann, I.-J., and Weidemann, V. 1972, *Ap. J.*, **178**, 427.
Sofia, S. 1971, *Nature*, **234**, 155.
Strittmatter, P. A., Robertson, J. W., and Faulkner, D. J. 1970, *Astr. and Ap.*, **5**, 426.
Sweet, P. A., and Roy, A. E. 1953, *M.N.R.A.S.*, **113**, 701.
Tayler, R. J. 1973, *M.N.R.A.S.*, **165**, 39.
Wasiutyński, J. 1946, *Ap. Norvegica*, **4**, 1.
Weir, A. D. 1975, *Mém. Soc. Roy. Sci. Liège*, **8**, 37.
Whelan, J. A. J. 1972, *M.N.R.A.S.*, **160**, 63.
Whelan, J. A. J., Papaloizou, J. C. B., and Smith, R. C. 1971, *M.N.R.A.S.*, **152**, 9P.
Zahn, J.-P. 1974, in *Stellar Instability and Evolution*, ed. P. Ledoux *et al.* (Dordrecht: Reidel), p. 185.

A. S. ENDAL: Department of Physics, Cardwell Hall, Kansas State University, Manhattan, KS 66506

S. SOFIA: Code SG, NASA Headquarters, Washington, DC 20546